SUPERCONDUCTIVITY

10.1126/sciadv.1501657

Inverse correlation between quasiparticle mass and T_c in a cuprate high-T_c superconductor

Carsten Putzke,[1] Liam Malone,[1] Sven Badoux,[2] Baptiste Vignolle,[2] David Vignolles,[2] Wojciech Tabis,[2,3] Philip Walmsley,[1] Matthew Bird,[1] Nigel E. Hussey,[4] Cyril Proust,[2] Antony Carrington[1]*

Close to a zero-temperature transition between ordered and disordered electronic phases, quantum fluctuations can lead to a strong enhancement of electron mass and to the emergence of competing phases such as superconductivity. A correlation between the existence of such a quantum phase transition and superconductivity is quite well established in some heavy fermion and iron-based superconductors, and there have been suggestions that high-temperature superconductivity in copper-oxide materials (cuprates) may also be driven by the same mechanism. Close to optimal doping, where the superconducting transition temperature T_c is maximal in cuprates, two different phases are known to compete with superconductivity: a poorly understood pseudogap phase and a charge-ordered phase. Recent experiments have shown a strong increase in quasiparticle mass m^* in the cuprate $YBa_2Cu_3O_{7-\delta}$ as optimal doping is approached, suggesting that quantum fluctuations of the charge-ordered phase may be responsible for the high-T_c superconductivity. We have tested the robustness of this correlation between m^* and T_c by performing quantum oscillation studies on the stoichiometric compound $YBa_2Cu_4O_8$ under hydrostatic pressure. In contrast to the results for $YBa_2Cu_3O_{7-\delta}$, we find that in $YBa_2Cu_4O_8$, the mass decreases as T_c increases under pressure. This inverse correlation between m^* and T_c suggests that quantum fluctuations of the charge order enhance m^* but do not enhance T_c.

INTRODUCTION

In a variety of systems such as organics, heavy fermions, iron pnictides, and copper oxides (cuprates), superconductivity is found in close proximity to an antiferromagnetic phase (*1*–*4*). Starting with the non-superconducting parent antiferromagnetic phase, because the material properties are tuned by the application of pressure or chemical doping, the magnetic ordering temperature T_N decreases. The doping/pressure where T_N extrapolates to zero is known as a quantum critical point (QCP). In many systems, the superconducting transition temperature T_c is maximal close to the doping/pressure where the QCP is located, thus suggesting an intimate connection between the two. Close to a QCP, quantum fluctuations between the ordered magnetic phase and the disordered paramagnetic phase become strong, and if such fluctuations produce electron pairing, this may enhance T_c. The strong fluctuations also affect the normal-state properties, causing a strong increase in quasiparticle mass and in the non-Fermi liquid behavior of the transport properties. Hence, close to a QCP, the normal-state entropy is increased, and this too could provide a boost for T_c (*1*, *3*).

The applicability of such a quantum critical scenario to cuprate superconductors is somewhat debatable because in these materials, T_c is zero close to the QCP of the antiferromagnetic phase. Instead, T_c is maximal close to the end points of two other phases: the pseudogap phase and the charge density wave (CDW) phase. Whether there is a QCP at the end points of either of these phases is unclear, as is their exact position (*5*, *6*). The nature and origin of the long-established pseudogap phase, which can be characterized as a depression of the density of states at the Fermi level (*7*) and a decoherence of quasiparticles on certain parts of the Fermi surface (*8*), are not well understood. In contrast, the more recently discovered CDW phases (*9*–*11*) seem to be more conventional, although many aspects, such as the microscopic mechanism of their formation and their variation with pressure, still need to be clarified. There are two distinct CDW phases. One phase, which is essentially two-dimensional, forms independently of a magnetic field below $T \sim 150$ K (*10*, *11*), whereas a second distinct three-dimensional order forms for fields above $T \sim 15$ T and below $T \sim 60$ K (*9*, *12*, *13*).

A CDW produces an additional periodic potential, which reduces the size of the Brillouin zone and folds the Fermi surface into small Fermi pockets. There is compelling evidence that a CDW-induced Fermi surface reconstruction is responsible for the small Fermi surface pockets, which are observed in quantum oscillation (QO) measurements (*14*), so QOs give a precise way of characterizing how the normal-state electronic structure is affected by the CDW. In particular, from the thermal damping of the QO amplitude, the quasiparticle mass m^* can be inferred. m^* is directly related to the renormalization of the band structure close to the Fermi level coming from the interaction of the electrons with collective excitations such as phonons or spin/CDW fluctuations.

Recently, the variation of m^* in the cuprate $YBa_2Cu_3O_{7-\delta}$ (Y123) was measured over a wide range of hole doping (n_p) (*15*, *16*). A dome-shaped variation of $(m^*)^{-1}$ versus n_p was found, with $(m^*)^{-1}$ extrapolating to zero at two points, $n_{p\,c1} \simeq 0.08$ and $n_{p\,c2} \simeq 0.18$. This is suggestive of QCPs close to $n_{p\,c1}$ and $n_{p\,c2}$ and because the latter value is close to the value ($n_p \simeq 0.165$) where T_c is maximal (*17*), this may indicate that the interactions responsible for the mass enhancement also give rise to the high-T_c superconductivity (*18*). It is natural to assume that these interactions are the fluctuations of the CDW, although additional coupling to the pseudogap fluctuations is also a possible cause (*15*).

[1]H. H. Wills Physics Laboratory, University of Bristol, Tyndall Avenue, Bristol BS8 1TL, UK. [2]Laboratoire National des Champs Magnétiques Intenses, CNRS-INSA-UJF-UPS, 31400 Toulouse, France. [3]AGH University of Science and Technology, Faculty of Physics and Applied Computer Science, aleja Adama Mickiewicza 30, 30-059 Krakow, Poland. [4]High Field Magnet Laboratory (HFML-EMFL), Radboud University, Toernooiveld 7, 6525 ED Nijmegen, Netherlands.
*Corresponding author. E-mail: a.carrington@bristol.ac.uk

Although chemical doping (for example, by changing the oxygen content δ in Y123) is the most widely used method of tuning the properties of cuprates, pressure is another available tuning parameter, and indeed the highest transition temperatures are achieved under high pressure (*19*). Here, we report measurements of QOs under high pressure in the stoichiometric cuprate $YBa_2Cu_4O_8$ (Y124). This allows us to study how the electronic correlations evolve as T_c is increased with pressure in a single sample with fixed stoichiometry.

Y124 has a structure similar to that of Y123 but with a double copper oxide chain layer. Unlike Y123, in Y124 the oxygen stoichiometry is fixed and thus cannot be used to change the doping or T_c. However, the application of hydrostatic pressure to Y124 leads to a strong increase in T_c by 5.5 K/GPa at low pressure (*20*). T_c increases from 79 K at ambient pressure [where $n_p \simeq 0.13(1)$ (*21*)] to ~105 K at ~8 GPa (*22*, *23*) at which point it undergoes a structural phase transition and becomes nonsuperconducting (*24*, *25*). Although direct x-ray or nuclear magnetic resonance (NMR) evidence for the existence of a CDW in Y124 remains missing to date, its existence is likely, as the transport properties (*26*) show features similar to those in Y123, which have been ascribed to CDW formation. Furthermore, QOs with a frequency similar to those seen in Y123 have been observed in Y124 (*21*, *27*), strongly suggesting that a similar CDW-driven Fermi surface reconstruction occurs.

RESULTS

Figure 1 shows ambient-pressure measurements of the *c*-axis resistivity ρ_c in a pulsed magnetic field of up to 67 T applied parallel to the *c* axis (perpendicular to the CuO_2 planes) of a single-crystal sample of Y124. Shubnikov–de Haas QOs in the resistance are clearly visible in the raw data above ~52 T but are more clearly seen in $d\rho_c/dH$ (Fig. 1, inset). The frequency *F* (in the inverse field) of these oscillations is 640 T, consistent with previous reports (*21*, *27*). The size of the oscillations is remarkably reproducible between different crystals (fig. S1). By fitting the temperature dependence of the oscillation amplitude, the quasiparticle mass can be extracted (Fig. 1B). We find a value of $m^* = 1.80(5)$ (in units of free electron mass). A value of $m^* = 1.9(1)$ was measured in two further samples (fig. S2). This is consistent with another recent study (*28*); however, older measurements (*21*, *27*) found larger values of m^*, but the errors were considerably larger than in the present work (see also Materials and Methods).

This same sample was then transferred to a nonmetallic pressure cell (*29*). Measurements of $\rho_c(H,T)$ at different applied pressures (*p*) up to $p = 0.84$ GPa are shown in Fig. 2. Because of the larger bore of the magnet used for the pressure cell measurements, the maximum field here was 58 T. At room temperature, ρ_c decreases linearly with increasing pressure (fig. S3A), and this decrease is essentially independent of temperature down to $T_c(H = 0)$ (fig. S3B). However, when superconductivity is suppressed by field at low temperatures, a markedly different behavior emerges. As can be seen in Fig. 2, both the magnitude of the resistivity and its slope ($d\rho_c/dH$) at 2.5 K and 50 T almost double between $p = 0$ and $p = 0.37$ GPa (the lowest pressure that we are able to apply), which suggests that, at low temperatures, the size of magnetoresistance significantly increases with the application of pressure, presumably due to an increase in the mean free path on some parts of the Fermi surface. This result was reproduced in three samples.

We were able to observe QOs at all pressures. The oscillatory part of the magnetoresistance at a fixed temperature of 2.5 K is shown in

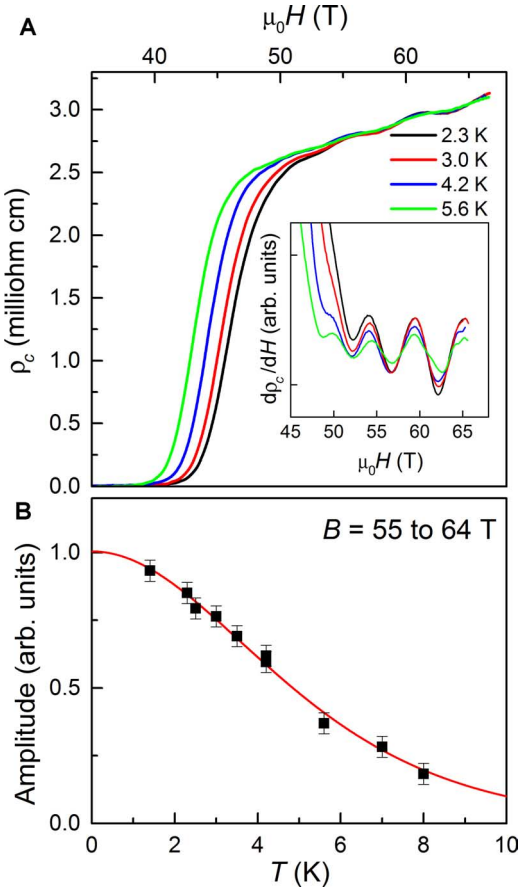

Fig. 1. Temperature-dependent magnetoresistance of Y124. (**A**) *c*-axis resistivity at different temperatures, measured up to $\mu_0 H = 67$ T. The inset shows the derivative $d\rho_c/dH$ to emphasize the Shubnikov–de Haas QOs. (**B**) Temperature dependence of the QO amplitude. The red line shows a fit to the Lifshitz-Kosevich expression (see Materials and Methods) giving a quasiparticle mass $m^* = (1.80 \pm 0.05)\, m_e$ (where m_e is the free electron mass).

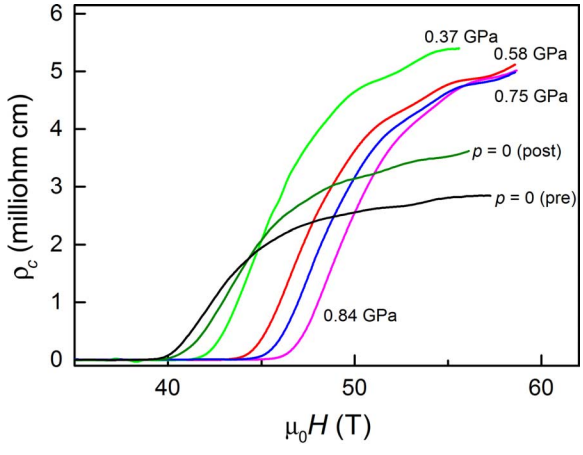

Fig. 2. Magnetoresistance of Y124 at various pressures at $T = 2.5$ K. Data for $p = 0$ are shown both before the pressure was applied and after it was removed.

Fig. 3A. The relative oscillation amplitude ($\Delta\rho_c/\rho_c$) increases by around a factor of 2 between $p = 0$ and $p = 0.37$ GPa but then remains approximately constant as pressure is increased further. There is a shift in the phase of the oscillations as a function of p, which is consistent with a small shift of frequency, equivalent to the Fermi surface area changing by ~10% between 0 and 0.84 GPa (Fig. 3B). Again, the change is largest between 0 and 0.37 GPa and then varies linearly with further increase in pressure. On depressurization to $p = 0$ after the highest pressure, $\rho_c(T)$ for $T > T_c(H = 0)$ approximately returns to the values before pressurization (fig. S3) as does T_c, but the magnetoresistance at low temperatures (Fig. 2) remains larger. The phase shift in the depressurized ($p = 0$) state follows the linear relation found at higher pressures (Fig. 3B).

The temperature dependence of the oscillation amplitudes at the different pressures, along with the fits to determine the effective masses, is shown in Fig. 4A. The mass found at low pressures measured inside the pressure cell is the same as the value measured outside the cell where the sample is in contact with liquid helium at low temperatures. This shows that there are no systematic errors in the mass determination introduced by the pressure cell. Figure 4B shows a central result of this paper, namely, that the effective mass strongly decreases with pressure and hence has an inverse correlation with T_c.

DISCUSSION

In Fig. 5, we make a comparison between the effective mass and T_c in Y123 (where T_c is varied by changing the oxygen content δ) and in Y124 (where T_c is varied by pressure). The inverse of the mass is plotted to emphasize the almost linear relation between $(m^*)^{-1}$ and n_p found in Y123 close to the two putative QCPs (*15*). It is clear that in Y124, the opposite trend is observed such that the effective mass decreases as T_c increases toward the maximum.

In interpreting these results, it is necessary to discuss how the physical properties of Y124 are changed under pressure and the mechanism of mass enhancement. The main effect of hydrostatic pressure on the structure of Y124 is to decrease all three lattice parameters, but the distance from the CuO_2 plane to the apical oxygen reduces twice as rapidly as the *c*-axis parameter itself (*30*). This distance is correlated with n_p in Y123 (*17*, *31*) and hence suggests that n_p increases with increasing pressure in Y124 (*30*). This is supported by experiments showing that, with increasing pressure, room temperature resistivity and thermoelectric power (*32*, *33*) both decrease as does the pseudogap temperature, as measured by NMR Knight shift (*34*). It is also supported by our observation that the QO frequency in Y124 increases with pressure. In Y123, an approximately linear increase in F has been found with increasing n_p (*35*), and it is interesting to note that, when plotted against T_c, the data for $F(p)$ in Y124 form an almost-perfect linear continuation of the increase in F with n_p for Y123 (fig. S4).

Quantitative estimates of dn_p/dp (Supplementary Materials) and the fact that the maximum T_c in Y124 and Y123 under pressure is ~105 K (which is considerably higher than the maximum T_c of ~94 K that can be achieved by changing δ in Y123 alone) suggest that charge transfer is not the only pressure-induced effect that increases T_c. It has recently been proposed that an important additional effect could be weakening of CDW order with pressure (*36*). Because the CDW competes for states with superconductivity, as evidenced by the observed dip in T_c and upper critical field H_{c2} at the value of n_p where the CDW is strongest (*37*), then T_c may be enhanced if the CDW is weakened. Although weakening of the CDW order remains a possibility at higher pressures, we find no decrease in the amplitude of the QO with increasing p (Fig. 3A). This strongly suggests that there is no significant decoherence of the high-field CDW for $p < 0.84$ GPa. The increase in QO amplitude with increased p indicates an increase in the CDW coherence.

As T_c increases linearly with p (<4 GPa), it is unlikely that the anomalously large effect of the initial pressurization on F (Fig. 3B)

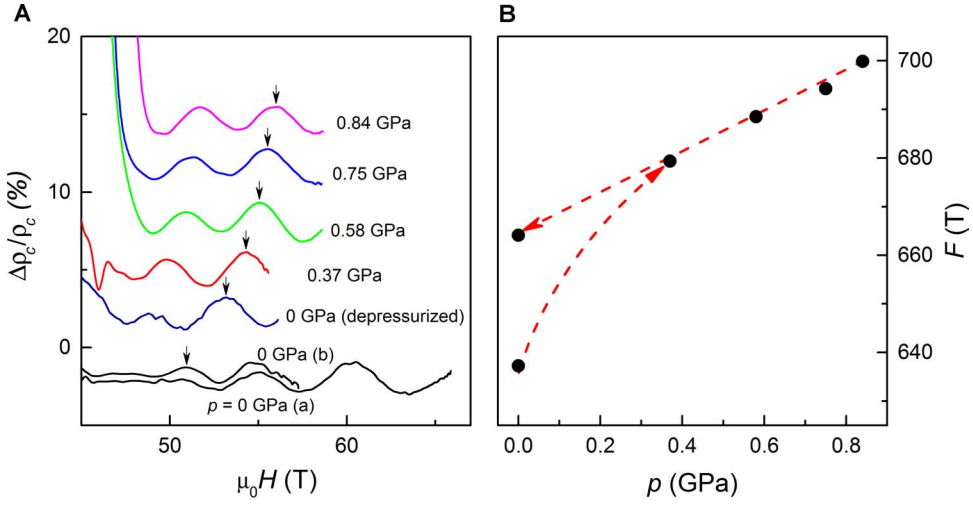

Fig. 3. Oscillatory part of resistance versus field for different pressures at $T = 2.5$ K. (**A**) Three curves for $p = 0$ GPa. (a) and (b) were measured outside the pressure cell: (a) in a 70-T coil and (b) in the same 60-T coil as the pressure cell measurements. The third curve is the result at $p = 0$ after depressurizing the cell. The arrows mark the position of a local maximum B_{max} in $\Delta\rho_c/\rho_c$. The curves have been offset vertically for clarity. (**B**) Evolution of the QO frequency with pressure. For $p = 0$ (before pressurization), the frequency was taken from a direct fit to $\sin(2\pi F/B + \phi)$, then the changes in the frequency as p is varied are inferred from B_{max}. Similar changes in F were also found by fitting each curve (as for $p = 0$) but at a higher noise level.

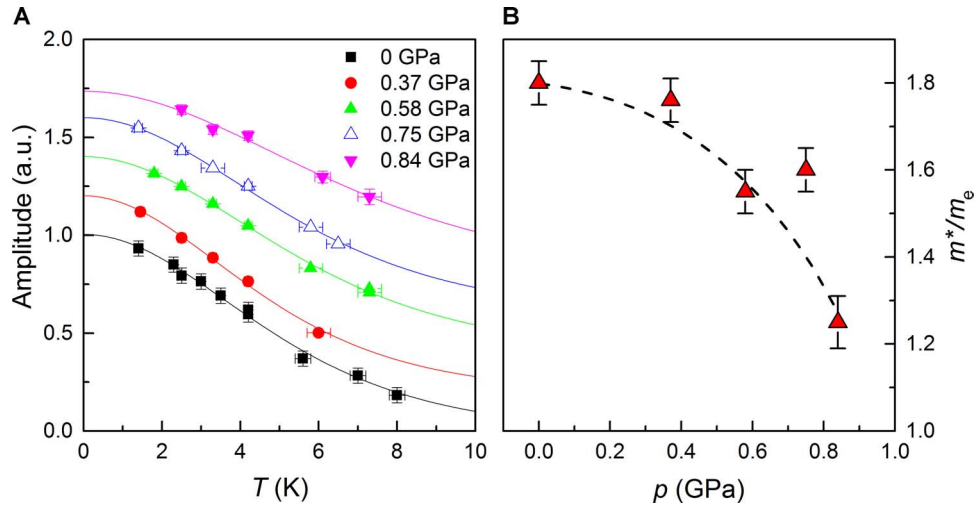

Fig. 4. Quasiparticle effective mass in Y124 under hydrostatic pressure. (**A**) Amplitude of QOs as a function of temperature. The curves have been offset vertically for clarity. The solid lines are fits to the Lifshitz-Kosevich formula. The field windows used are given in table S1. (**B**) Variation of quasiparticle mass with pressure extracted from the fits. The dashed line is a guide to the eye. a.u., arbitrary units.

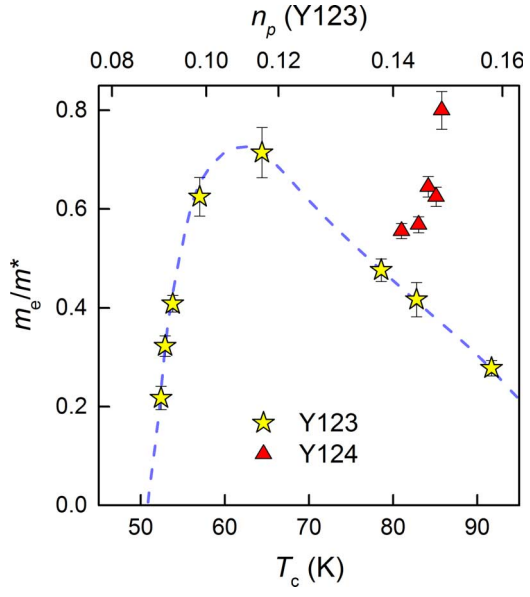

Fig. 5. Quasiparticle mass of Y124 compared to Y123 plotted versus T_c. The top scale shows the hole doping level for Y123 (*17*). Data for Y123 are taken from Ramshaw *et al.* (*15*) and the references therein. The dashed line is a guide to the eye.

and the magnitude of the magnetoresistance (Fig. 2) are mainly due to charge transfer. More likely, it results from an increase in the order of any residual vacancies in the material. This would lead to an increase in the mean free path and, in turn, the QO amplitude and the size of the magnetoresistance. When the pressure is removed, this increased order may persist, giving rise to the observed hysteresis of $F(p)$ (Fig. 3B) and the magnetoresistance. However, we find that this increased order does not have any significant effect on m^* (Fig. 4) and so does not affect our central conclusion.

The increase in m^* in Y123 close to optimal doping (*15*) could be interpreted as resulting from enhanced coupling to fluctuations in either CDW or pseudogap order because these modes would be expected to soften close to their end points. Our key finding is that in Y124, m^* decreases as T_c increases under pressure, which clearly demonstrates that the enhancement found for m^* in Y123 as δ is reduced, increasing T_c toward optimal, is not universal. Rather, it suggests that the approximate coincidence of $n_{p\ c2}$ (the doping where $1/m^*$ extrapolates to 0 in Y123) and the doping where T_c is maximal are accidental, so there is no causal connection between the fluctuations giving rise to the mass enhancement and T_c. The decrease in m^* in Y124 could be interpreted as resulting from a decrease in CDW fluctuations caused by the pressure-induced structural changes. For example, the reduction in *c*-axis length caused by increasing pressure might help stabilize the high-field CDW phase where three-dimensional coupling is important and hence increases the CDW coherence, thereby reducing the mass enhancing fluctuations. Elucidation of the microscopic changes will require a structural study of the CDW at high pressure. Our results suggest that the proximity of the CDW end point to the maximum in T_c with doping is coincidental and that, therefore, quantum fluctuations of the CDW order do not boost T_c in cuprates.

MATERIALS AND METHODS

Crystal growth and characterization

Crystals of Y124 were grown from a mixture of Y123 powder and CuO_2 in a KOH flux (*38*). The obtained crystals had a typical size of 200 × 200 × 100 μm, with the shortest dimension being along the *c* axis. The composition was checked using x-ray diffraction, and the lattice parameters were found to be in agreement with previous reports. The samples displayed a sharp superconducting transition with T_c = 79 K. For resistance measurements, four contacts were made (two each on the top and bottom faces) using evaporated gold pads, which were annealed onto the sample at 500°C and then contacted with DuPont 4929 silver epoxy. Typical contact resistances were <0.1 Ω at

4.2 K. In zero field, resistance was measured using a standard low-frequency lock-in amplifier method, and in pulsed field, resistance was measured using a numerical lock-in digitization technique typically operating at 54 kHz. Resistance-versus-temperature curves are shown in fig. S3B. R_c shows metallic behavior at low temperatures and is similar to the results reported by Hussey *et al.* (*39*).

Pressure cell

A nonmagnetic pressure cell was used in the pulsed magnetic field system (*29*). Because of space limitations inside this cell, pressure was determined using the samples themselves as a manometer. Changes in the R_c values of the Y124 samples were measured in the nonmetallic cell at room temperature, and these results were compared to measurements performed in a different larger cell where the pressure was measured at low temperatures using a Pb manometer and at room temperature using the resistance of a manganin wire (*40*). In this second cell, it was verified, by *c*-axis resistivity measurements, that dT_c/dP was 5.5(5) K/GPa, in agreement with previous measurements (*20*).

Effective mass determination

QO data were analyzed by fitting the following function to the $R_c(B)$ data

$$R(B) = AB^{0.5}\exp(-\alpha/B)\sin(2\pi F/B+\phi) + a_0 + a_1B + a_2B^2 + a_3B^3 + a_4B^4 \quad (1)$$

The first part of the function represents the field-dependent part of the Lifshitz-Kosevich formula (*41*) for the QO amplitude in a three-dimensional metal at $T = 0$. We fit this to a short section of data (field ranges for each pressure are given in table S1) at the lowest temperature (typically $T = 1.4$ K) and determine α, F, and ϕ. These parameters are then left fixed, and the oscillation amplitude A was then determined as a function of temperature. A fourth-order polynomial (a_0 to a_4) was used to subtract the nonoscillatory background resistance. The temperature dependence of A was then fitted to the thermal damping factor $R_T = X/\sinh(X)$, $X = 2\pi^2 k_B m^* T/(e\hbar B)$ to extract the effective mass m^*. In this formula, B is set to the average inverse field in the field range fitted.

Thermometry in the pulsed magnetic field

To accurately determine the mass, it is necessary to accurately measure the sample temperature. This is not trivial in a pulsed-field system because the relatively high sample currents needed to obtain a sufficient signal-to-noise ratio produce heating at the sample contacts. These effects were minimized in our measurements by obtaining very low contact resistances (around 0.1 Ω) and having the sample in direct contact with liquid helium (for $T \leq 4.2$ K) for measurements outside of the pressure cell.

For measurement inside the pressure cell, the thermometer was mounted directly outside the cell. Tests using a miniature GeAu thermometer mounted inside the cell (attached to the sample) showed that the two thermometers were in thermal equilibrium provided that the resistive heating at the sample contacts was sufficiently low. The maximum current used for the resistivity measurements was selected so that this was always the case.

The strong increase in the H of the superconducting-normal transition with temperature was used as a second check of the temperature. The irreversibility field H_{irr}, defined as the field where the resistance first increases above the noise, varies linearly with T (fig. S5). The continuity of this linear behavior when the sample is inside the cell provides an important check that the sample temperature has been correctly determined.

Estimates of change in doping with pressure

A quantitative estimate of the change in n_p with p can be made using the magnitude of the room temperature *a*-axis thermoelectric power ($S^a_{290\ K}$). Using the data for Y124 in the study by Zhou *et al.* (*32*) along with the universal relation between n_p and $S^a_{290\ K}$ (*33*, *42*), we obtained $dn_p/dp = 2.3(6) \times 10^{-3}$ holes/GPa. A second estimate can be made using the pressure-dependent NMR Knight shift ^{17}K data for Y124 from Meissner *et al.* (*34*). Following Tallon *et al.* (*43*), we scaled the temperature axis by the pseudogap energy E_g so that the data for different pressures collapse onto a single curve and $^{17}K(T/E_g)$ is approximately constant for $T/E_g > 1$. For $p = 0$, we estimated $E_g = 350$ K, which is consistent with the *a*-axis resistivity $\rho_a(T)$ data (*39*). From this, we obtained $dn_p/dp = 3.6(4) \times 10^{-3}$ holes/GPa for $p \leq 4.2$ GPa, which is in reasonable agreement with the above estimate from $S^a_{290\ K}$. Taking the average of these two values and combining them with an estimate of dT_c/dn_p taken from Y123 at $n_p = 0.13$ (*17*) would predict that for Y124, $dT_c/dp = 2.7(5)$ K/GPa [that is, about two times smaller than the measured $dT_c/dp = 5.5(1)$ K/GPa] (*23*).

Although the quantitative precision of this estimate should be viewed with caution because the universal relations between $S^a_{290\ K}$ and n_p (*33*, *42*) and between E_g and n_p (*43*) may not hold under finite pressure, it is likely that there are other effects that increase T_c in addition to charge transfer.

In simple systems, the QO frequency F, which is proportional to the Fermi surface extremal cross section, can often be used to precisely determine the doping level. However, in cuprates, this has so far only been successfully demonstrated in the overdoped cuprate $Tl_2Ba_2CuO_{6+\delta}$ (*44*–*46*). For underdoped materials, the reconstruction of the Fermi surface complicates the analysis because the area of the reconstructed pocket will depend on the unknown details of the reconstructing potential, as well as n_p. In Y123, an approximately linear increase in F with increasing n_p (*35*) has been found. If we assume that dF/dn_p in Y124 is the same as in Y123 for $0.09 < n_p < 0.125$, then the slope dF/dp from the linear part of Fig. 3B would give $dn_p/dp = 1.0(2) \times 10^{-2}$ holes/GPa, which is around three times larger than the estimate from $S^a_{290\ K}(p)$. However, because it remains unknown how universal $F(n_p)$ is in cuprates, this estimate is probably the most uncertain.

SUPPLEMENTARY MATERIALS

Supplementary material for this article is available at http://advances.sciencemag.org/cgi/content/full/2/3/e1501657/DC1

Fig. S1. Sample dependence of zero-pressure QOs.
Fig. S2. Effective mass determination at $p = 0$ for two further samples.
Fig. S3. Pressure dependence of $\rho_c(T)$.
Fig. S4. Comparison of changes in QO frequency between Y123 and Y124.
Fig. S5. Temperature and pressure dependence of the irreversible field H_{irr}.
Table S1. Field windows used for the fitting of temperature-dependent QO amplitudes at various pressures, as shown in Fig. 4.

REFERENCES AND NOTES

1. S. Sachdev, B. Keimer, Quantum criticality. *Phys. Today* **64**, 29–35 (2011).
2. L. Taillefer, Scattering and pairing in cuprate superconductors. *Annu. Rev. Condens. Matter Phys.* **1**, 51–70 (2010).

3. T. Shibauchi, A. Carrington, Y. Matsuda, A quantum critical point lying beneath the superconducting dome in iron pnictides. *Annu. Rev. Condens. Matter Phys.* **5**, 113–135 (2014).
4. D. M. Broun, What lies beneath the dome? *Nat. Phys.* **4**, 170–172 (2008).
5. M. Hücker, N. B. Christensen, A. T. Holmes, E. Blackburn, E. M. Forgan, R. Liang, D. A. Bonn, W. N. Hardy, O. Gutowski, M. v. Zimmermann, S. M. Hayden, J. Chang, Competing charge, spin, and superconducting orders in underdoped $YBa_2Cu_3O_y$. *Phys. Rev. B* **90**, 054514 (2014).
6. S. Blanco-Canosa, A. Frano, E. Schierle, J. Porras, T. Loew, M. Minola, M. Bluschke, E. Weschke, B. Keimer, M. Le Tacon, Resonant x-ray scattering study of charge-density wave correlations in $YBa_2Cu_3O_{6+x}$. *Phys. Rev. B* **90**, 054513 (2014).
7. J. L. Tallon, J. W. Loram, The doping dependence of T^* — What is the real high-T_c phase diagram? *Physica C* **349**, 53–68 (2001).
8. A. Damascelli, Z. Hussain, Z.-X. Shen, Angle-resolved photoemission studies of the cuprate superconductors. *Rev. Mod. Phys.* **75**, 473–541 (2003).
9. T. Wu, H. Mayaffre, S. Krämer, M. Horvatić, C. Berthier, W. N. Hardy, R. Liang, D. A. Bonn, M.-H. Julien, Magnetic-field-induced charge-stripe order in the high-temperature superconductor $YBa_2Cu_3O_y$. *Nature* **477**, 191–194 (2011).
10. G. Ghiringhelli, M. Le Tacon, M. Minola, S. Blanco-Canosa, C. Mazzoli, N. B. Brookes, G. M. De Luca, A. Frano, D. G. Hawthorn, F. He, T. Loew, M. M. Sala, D. C. Peets, M. Salluzzo, E. Schierle, R. Sutarto, G. A. Sawatzky, E. Weschke, B. Keimer, L. Braicovich, Long-range incommensurate charge fluctuations in $(Y,Nd)Ba_2Cu_3O_{6+x}$. *Science* **337**, 821–825 (2012).
11. J. Chang, E. Blackburn, A. T. Holmes, N. B. Christensen, J. Larsen, J. Mesot, R. Liang, D. A. Bonn, W. N. Hardy, A. Watenphul, M. v. Zimmermann, E. M. Forgan, S. M. Hayden, Direct observation of competition between superconductivity and charge density wave order in $YBa_2Cu_3O_{6.67}$. *Nat. Phys.* **8**, 871–876 (2012).
12. T. Wu, H. Mayaffre, S. Krämer, M. Horvatić, C. Berthier, W. N. Hardy, R. Liang, D. A. Bonn, M.-H. Julien, Incipient charge order observed by NMR in the normal state of $YBa_2Cu_3O_y$. *Nat. Commun.* **6**, 6438 (2015).
13. S. Gerber, H. Jang, H. Nojiri, S. Matsuzawa, H. Yasumura, D. A. Bonn, R. Liang, W. N. Hardy, Z. Islam, A. Mehta, S. Song, M. Sikorski, D. Stefanescu, Y. Feng, S. A. Kivelson, T. P. Devereaux, Z.-X. Shen, C.-C. Kao, W.-S. Lee, D. Zhu, J.-S. Lee, Three-dimensional charge density wave order in $YBa_2Cu_3O_{6.67}$ at high magnetic fields. *Science* **350**, 949–952 (2015).
14. N. Doiron-Leyraud, C. Proust, D. LeBoeuf, J. Levallois, J.-B. Bonnemaison, R. Liang, D. A. Bonn, W. N. Hardy, L. Taillefer, Quantum oscillations and the Fermi surface in an underdoped high-T_c superconductor. *Nature* **447**, 565–568 (2007).
15. B. J. Ramshaw, S. E. Sebastian, R. D. McDonald, J. Day, B. S. Tan, Z. Zhu, J. B. Betts, R. Liang, D. A. Bonn, W. N. Hardy, N. Harrison, Quasiparticle mass enhancement approaching optimal doping in a high-T_c superconductor. *Science* **348**, 317–320 (2015).
16. S. E. Sebastian, N. Harrison, G. G. Lonzarich, Towards resolution of the Fermi surface in underdoped high-T_c superconductors. *Rep. Prog. Phys.* **75**, 102501 (2012).
17. R. Liang, D. A. Bonn, W. N. Hardy, Evaluation of CuO_2 plane hole doping in $YBa_2Cu_3O_{6+x}$ single crystals. *Phys. Rev. B* **73**, 180505 (2006).
18. C. Castellani, C. Di Castro, M. Grilli, Non-Fermi-liquid behavior and d-wave superconductivity near the charge-density-wave quantum critical point. *Z. Phys. B Condens. Matter* **103**, 137–144 (1996).
19. L. Gao, Y. Y. Xue, F. Chen, Q. Xiong, R. L. Meng, D. Ramirez, C. W. Chu, J. H. Eggert, H. K. Mao, Superconductivity up to 164 K in $HgBa_2Ca_{m-1}Cu_mO_{2m+2+\delta}$ (m=1,2, and 3) under quasihydrostatic pressures. *Phys. Rev. B* **50**, 4260–4263 (1994).
20. B. Bucher, J. Karpinski, E. Kaldis, P. Wachter, Strong pressure dependence of T_c of the new 80 K phase $YBa_2Cu_4O_{8+x}$. *Physica C* **157**, 478–482 (1989).
21. E. A. Yelland, J. Singleton, C. H. Mielke, N. Harrison, F. F. Balakirev, B. Dabrowski, J. R. Cooper, Quantum oscillations in the underdoped cuprate $YBa_2Cu_4O_8$. *Phys. Rev. Lett.* **100**, 047003 (2008).
22. E. N. Van Eenige, R. Griessen, R. J. Wijngaarden, J. Karpinski, E. Kaldis, S. Rusiecki, E. Jilek, Superconductivity at 108 K in $YBa_2Cu_4O_8$ at pressures up to 12 GPa. *Physica C* **168**, 482–488 (1990).
23. J. J. Scholtz, E. N. van Eenige, R. J. Wijngaarden, R. Griessen, Pressure dependence of T_c and H_{c2} of $YBa_2Cu_4O_8$. *Phys. Rev. B* **45**, 3077–3082 (1992).
24. A. Nakayama, Y. Onda, S. Yamada, H. Fujihisa, M. Sakata, Y. Nakamoto, K. Shimizu, S. Nakano, A. Ohmura, F. Ishikawa, Y. Yamada, Collapse of CuO double chains and suppression of superconductivity in high-pressure phase of $YBa_2Cu_4O_8$. *J. Phys. Soc. Jpn.* **83**, 093601 (2014).
25. M. Mito, T. Imakyurei, H. Deguchi, K. Matsumoto, H. Hara, T. Ozaki, H. Takeya, Y. Takano, Effective disappearance of the Meissner signal in the cuprate superconductor $YBa_2Cu_4O_8$ under uniaxial strain. *J. Phys. Soc. Jpn.* **83**, 023705 (2014).
26. D. LeBoeuf, N. Doiron-Leyraud, J. Levallois, R. Daou, J.-B. Bonnemaison, N. E. Hussey, L. Balicas, B. J. Ramshaw, R. Liang, D. A. Bonn, W. N. Hardy, S. Adachi, C. Proust, L. Taillefer, Electron pockets in the Fermi surface of hole-doped high-T_c superconductors. *Nature* **450**, 533–536 (2007).
27. A. F. Bangura, J. D. Fletcher, A. Carrington, J. Levallois, M. Nardone, B. Vignolle, P. J. Heard, N. Doiron-Leyraud, D. LeBoeuf, L. Taillefer, S. Adachi, C. Proust, N. E. Hussey, Small Fermi surface pockets in underdoped high temperature superconductors: Observation of Shubnikov–de Haas oscillations in $YBa_2Cu_4O_8$. *Phys. Rev. Lett.* **100**, 047004 (2008).
28. B. S. Tan, N. Harrison, Z. Zhu, F. Balakirev, B. J. Ramshaw, A. Srivastava, S. A. Sabok-Sayr, B. Dabrowski, G. G. Lonzarich, S. E. Sebastian, Fragile charge order in the non-superconducting ground state of the underdoped high-temperature superconductors. *Proc. Natl. Acad. Sci. U.S.A.* **112**, 9568–9572 (2015).
29. M. Nardone, A. Audouard, D. Vignolles, L. Brossard, Hydrostatic pressure anvil cell for electron transport measurements up to 1 GPa under high pulsed magnetic field at liquid helium temperatures. *Cryogenics* **41**, 175–178 (2001).
30. Y. Yamada, J. D. Jorgensen, S. Pei, P. Lightfoot, Y. Kodama, T. Matsumoto, F. Izumi, Structural changes of superconducting $YBa_2Cu_4O_8$ under high pressure. *Physica C* **173**, 185–194 (1991).
31. J. D. Jorgensen, B. W. Veal, A. P. Paulikas, L. J. Nowicki, G. W. Crabtree, H. Claus, W. K. Kwok, Structural properties of oxygen-deficient $YBa_2Cu_3O_{7-\delta}$. *Phys. Rev. B* **41**, 1863–1877 (1990).
32. J.-S. Zhou, J. B. Goodenough, B. Dabrowski, K. Rogacki, Transport properties of a $YBa_2Cu_4O_8$ crystal under high pressure. *Phys. Rev. Lett.* **77**, 4253–4256 (1996).
33. S. D. Obertelli, J. R. Cooper, J. L. Tallon, Systematics in the thermoelectric power of high-T_c oxides. *Phys. Rev. B* **46**, 14928–14931 (1992).
34. T. Meissner, S. K. Goh, J. Haase, G. V. M. Williams, P. B. Littlewood, High-pressure spin shifts in the pseudogap regime of superconducting $YBa_2Cu_4O_8$ as revealed by ^{17}O NMR. *Phys. Rev. B* **83**, 220517 (2011).
35. B. Vignolle, D. Vignolles, M.-H. Julien, C. Proust, From quantum oscillations to charge order in high-T_c copper oxides in high magnetic fields. *C. R. Phys.* **14**, 39–52 (2013).
36. O. Cyr-Choinière, D. LeBoeuf, S. Badoux, S. Dufour-Beauséjour, D. A. Bonn, W. N. Hardy, R. Liang, N. Doiron-Leyraud, L. Taillefer, Suppression of charge order by pressure in the cuprate superconductor $YBa_2Cu_3O_y$: Restoring the full superconducting dome. arXiv:1503.02033 (2015).
37. G. Grissonnanche, O. Cyr-Choinière, F. Laliberté, S. R. de Cotret, A. Juneau-Fecteau, S. Dufour-Beauséjour, M.-È. Delage, D. LeBoeuf, J. Chang, B. J. Ramshaw, D. A. Bonn, W. N. Hardy, R. Liang, S. Adachi, N. E. Hussey, B. Vignolle, C. Proust, M. Sutherland, S. Krämer, J.-H. Park, D. Graf, N. Doiron-Leyraud, L. Taillefer, Direct measurement of the upper critical field in cuprate superconductors. *Nat. Commun.* **5**, 3280 (2014).
38. G. L. Sun, Y. T. Song, C. T. Lin, Investigation of $YBa_2Cu_4O_8$ single crystal growth by KOH flux. *Supercond. Sci. Technol.* **21**, 125001 (2008).
39. N. E. Hussey, K. Nozawa, H. Takagi, S. Adachi, K. Tanabe, Anisotropic resistivity of $YBa_2Cu_4O_8$: Incoherent-to-metallic crossover in the out-of-plane transport. *Phys. Rev. B* **56**, R11423(R) (1997).
40. C.-y. Wang, Electrical resistance of manganin coil to 7 kbar and 200°C. *Rev. Sci. Instrum.* **38**, 24 (1967).
41. D. Shoenberg, *Magnetic Oscillations in Metals* (Cambridge Univ. Press, Cambridge, 1984), 570 pp.
42. J. L. Tallon, C. Bernhard, H. Shaked, R. L. Hitterman, J. D. Jorgensen, Generic superconducting phase behavior in high-T_c cuprates: T_c variation with hole concentration in $YBa_2Cu_3O_{7-\delta}$. *Phys. Rev. B Condens. Matter* **51**, 12911–12914 (1995).
43. J. L. Tallon, J. W. Loram, G. V. M. Williams, J. R. Cooper, I. R. Fisher, J. D. Johnson, M. P. Staines, C. Bernhard, Critical doping in overdoped high-T_c superconductors: A quantum critical point? *Phys. Status Solidi B* **215**, 531–540 (1999).
44. B. Vignolle, A. Carrington, R. A. Cooper, M. M. J. French, A. P. Mackenzie, C. Jaudet, D. Vignolles, C. Proust, N. E. Hussey, Quantum oscillations in an overdoped high-T_c superconductor. *Nature* **455**, 952–955 (2008).
45. A. F. Bangura, P. M. C. Rourke, T. M. Benseman, M. Matusiak, J. R. Cooper, N. E. Hussey, A. Carrington, Fermi surface and electronic homogeneity of the overdoped cuprate superconductor $Tl_2Ba_2CuO_{6+\delta}$ as revealed by quantum oscillations. *Phys. Rev. B* **82**, 140501 (2010).
46. P. M. C. Rourke, A. F. Bangura, T. M. Benseman, M. Matusiak, J. R. Cooper, A. Carrington, N. E. Hussey, A detailed de Haas–van Alphen effect study of the overdoped cuprate $Tl_2Ba_2CuO_{6+\delta}$. *New J. Phys.* **12**, 105009 (2010).

Acknowledgments: We thank J. Cooper, S. Friedemann, J. Tallon, and L. Taillefer for useful discussions. **Funding:** This work was supported by the Engineering and Physical Sciences Research Council (grant no. EP/K016709/1). A portion of this work was performed at the Laboratoire National de Champs Magnétiques Intenses, which is supported by the French National Research Agency (ANR) SUPERFIELD, the European Magnetic Field Laboratory, and the LABEX NEXT. We also acknowledge the support of the High Field Magnet Laboratory, Radboud University Fundamental Research on Matter. **Author contributions:** The experiment

was conceived by A.C., N.E.H., C. Putzke, and C. Proust. QO experiments were performed in Toulouse by C. Putzke, L.M., S.B., D.V., B.V., W.T., A.C., and C. Proust. The samples were grown and characterized by P.W., M.B., and C. Putzke. The paper was written by A.C. and C. Putzke with input from all of the co-authors. **Competing interests:** The authors declare that they have no competing interests. **Data and materials availability:** All data needed to evaluate the conclusions in the paper are present in the paper and/or the Supplementary Materials. Additional data related to this paper may be requested from the authors. Raw resistance versus field or resistance versus temperature data for all figures can be found at doi:10.5523/bris.p6wv6g0eoh3t1fd2d4fjujuno.

Submitted 17 November 2015
Accepted 28 January 2016
Published 18 March 2016
10.1126/sciadv.1501657

Citation: C. Putzke, L. Malone, S. Badoux, B. Vignolle, D. Vignolles, W. Tabis, P. Walmsley, M. Bird, N. E. Hussey, C. Proust, A. Carrington, Inverse correlation between quasiparticle mass and T_c in a cuprate high-T_c superconductor. *Sci. Adv.* **2**, e1501657 (2016).

ScienceAdvances
AAAS

Inverse correlation between quasiparticle mass and T_C in a cuprate high-T_C superconductor

Carsten Putzke, Liam Malone, Sven Badoux, Baptiste Vignolle, David Vignolles, Wojciech Tabis, Philip Walmsley, Matthew Bird, Nigel E. Hussey, Cyril Proust and Antony Carrington (March 18, 2016)

Sci Adv 2016, 2:.
doi: 10.1126/sciadv.1501657